Acta Materialia 225 (2022) 117558

Contents lists available at ScienceDirect

Acta Materialia

journal homepage: www.elsevier.com/locate/actamat

Role of point defects in the formation of relaxor ferroelectrics

Zhengkai Hong[a], Xiaoqin Ke[a,*], Dong Wang[a], Sen Yang[a,*], Xiaobing Ren[a,b], Yunzhi Wang[c]

[a] School of Physics, MOE Key Laboratory for Nonequilibrium Synthesis and Modulation of Condensed Matter, Frontier Institute of Science and Technology, State Key Laboratory for Mechanical Behavior of Materials, Xi'an Jiaotong University, Xi'an 710049, China
[b] Ferroic Physics Group, National Institute for Materials Science, Tsukuba, 305-0047 Ibaraki, Japan
[c] Department of Materials Science and Engineering, The Ohio State University, Columbus, OH 43210, USA

ARTICLE INFO

Article history:
Received 4 July 2021
Revised 11 October 2021
Accepted 11 December 2021
Available online 13 December 2021

ABSTRACT

Relaxor ferroelectrics are engineered by doping a large amount of point defects into normal ferroelectrics. The point defects create nanoscale compositional heterogeneity, which in turn lead to local Curie temperature (T_C) variation and random local electric and strain fields. However, it is still unclear about the individual roles played by each of these effects in converting a normal ferroelectric into a relaxor. In this study we distinguish these effects by carryout computer simulations using the phase field method. We find that although both the local-field and local-T_C effects could lead to the formation of nanodomains in relaxors, it is the former that leads to the appearance of Burns temperature T_B, the latter that leads to the appearance of the intermediate temperature T^*, and a combination of the two allows one to model all three characteristic temperatures of a relaxor reported in experiments: T_B, T^* and the freezing temperature T_f. This work unravels the roles of point defects in the formation of relaxor ferroelectrics and offers deep microscopic insight into relaxors.

1. Introduction

Relaxor ferroelectrics exhibit many unique properties including high dielectric permittivity over a wide temperature range, large electrostrictive strain with small-hysteresis and ultrahigh piezoelectric coefficients [1–3]. Due to these outstanding properties, relaxors have become indispensable in a wide range of key technological applications such as capacitors, actuators and sensors.

Relaxors are usually produced by doping a sufficient amount of point defects into normal ferroelectrics, such as La^{3+} doped $PbZr_xTi_{1-x}O_3$, [4]. Zr^{4+} doped $BaTiO_3$ [5] and Mg^{2+} and Nb^{5+} doped $PbTiO_3$ (PT-*x*PMN) [6]. These point defects are randomly distributed in the solid solutions and thus inevitably lead to compositional heterogeneity at nanoscale [1,7,8]. There are two possible effects associated with such nanoscale compositional heterogeneity: the local Curie temperature (T_C) variation arising from the composition-dependence of T_C, and the local electric and strain field effect arising respectively from the charge imbalance and atomic size mismatch caused by the point defects. The existing models have ascribed the formation of relaxors in various doped ferroelectric systems to either the local-T_C effect [9–13]. or the local-field effect [14–18]. However, it is still unclear about the unique roles played by each of these two effects in leading to the unique properties of relaxors, which creates difficulties for selecting the "right" dopants to optimize either the local-field effect, the local-T_C effect, or an optimal combination of the two effects. For example, three characteristic temperatures [19] (Burns temperature (T_B), [20] intermediate temperature (T^*) [21,22] and freezing temperature (T_f)) have been reported experimentally for perovskite-structured relaxors but it is elusive how these characteristic temperatures are related to the above two effects of point defects.

In this study we model the formation process of relaxors by considering both the local-T_C and local-field effects of point defects in phase field simulations. We are able to predict all three characteristic temperatures (T_B, $T^*$and T_f) observed in experiments for relaxors. More importantly, we find that it is the local-field effect that leads to the appearance of the Burns temperature T_B, it is the local-T_C effect that leads to the appearance of the intermediate temperature T^*, and it is the combination of the two that allows us to model all three characteristic temperatures. The simulations also revealed the domain structure evolution process of relaxors during cooling. These findings could deepen our understanding on the roles of point defects in the formation of relaxors and could guide the design of relaxors.

2. Phase field models

The system studied in this work is a model ferroelectric system with cubic (C)-tetragonal (T) transition at T_C doped with non-

* Corresponding authors.
E-mail addresses: kexiaoqin@xjtu.edu.cn (X. Ke), yangsen@xjtu.edu.cn (S. Yang).

https://doi.org/10.1016/j.actamat.2021.117558
1359-6454/

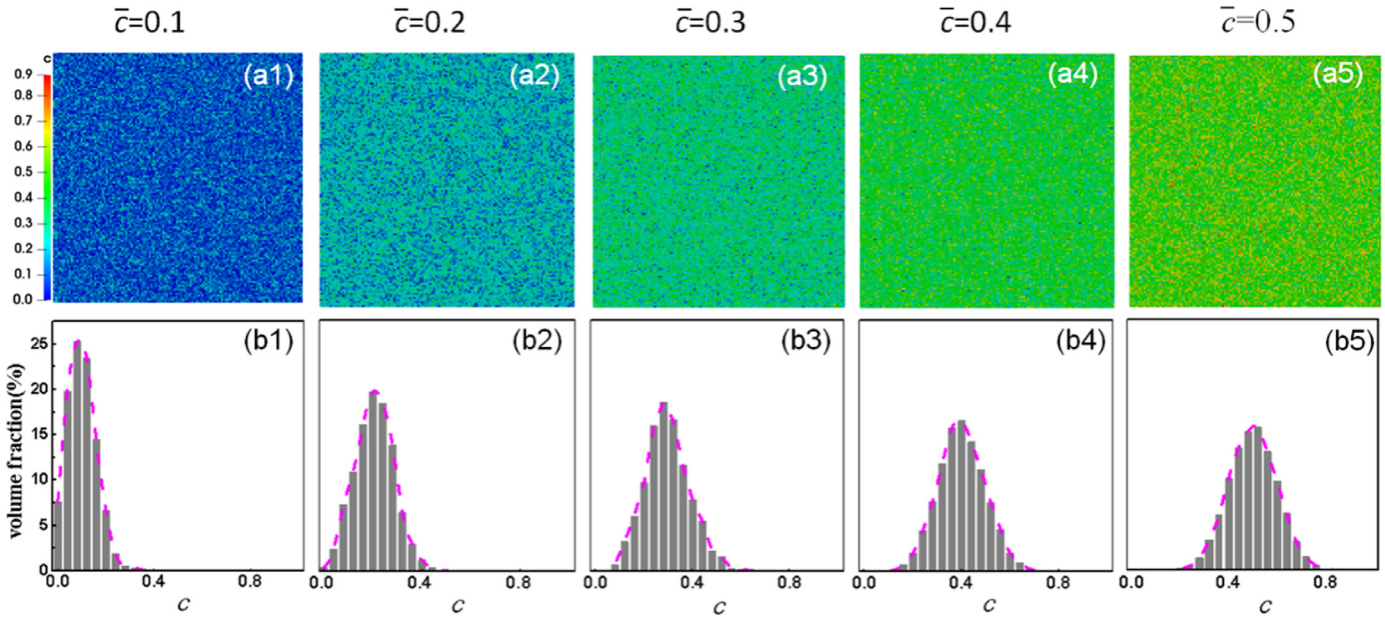

Fig. 1. (a1)-(a5) the spatial distribution of defect concentration for samples with different $\bar{c}$; (b1)-(b5) the volume fraction of grid points with different c.

ferroelectric heterovalent point defects. The average concentration of point defects is$\bar{c}$. The point defects are randomly distributed in the system and thus their concentration, c, at different grid points could be different from $\bar{c}$. Fig. 1(a1)-(a5) gives the spatial distribution of local defect concentration c for samples with different $\bar{c}$ and Fig. 1(b1)-(b5) calculates the volume fraction of grid points with different c for each sample. The point defects can create large local-field effect due to their heterovalent nature and can create large local-T_C effect due to their non-ferroelectric nature. The Curie temperature (T_C) of ferroelectric materials normally decrease with the increase of the concentration of non-ferroelectric defects and exhibit a nearly linear relationship with defect concentration c [23–26]. For simplicity, here the local Curie temperature is assumed to decrease linearly with local c at each gird point, i.e., $T_c = T_c^{00} - bc$ (T_C^{00} and b are both constants). The strength of local electric field is assumed to increase linearly with local c, i.e., $|E_{local}|$=λc where λ is a constant. And the direction of the local electric field is assumed to be random. Thus, the mean value of the local electric field is zero [27,28].

The domain microstructure of this doped ferroelectric system is described by spatial-dependent distribution of spontaneous polarization $\boldsymbol{P}$=[P_1,P_2,P_3]. The total free energy of the system can be written as the sum of four terms as shown below [29,30]: $F = \int_V (f_{bulk} + f_{grad} + f_{elec} + f_{elas})dV$,where V is the volume, f_{bulk}, f_{grad}, f_{elec}, f_{elas} are the bulk free energy density, the gradient energy density, the electrostatic energy density and the elastic energy density, respectively. f_{bulk}, f_{grad}, f_{elec}, f_{elas} are all written as a function of polarization **P**. The bulk free energy density, f_{bulk}, is approximated by a 6th order Landau polynomial:

$$\begin{aligned} f_{bulk} = {} & A_1 \sum_{i=1}^{3} P_i^2 + A_{11} \sum_{i=1}^{3} P_i^4 + A_{111} \sum_{i=1}^{3} P_i^6 \\ & + A_{12} \sum_{i,j=1,2,3}^{i\neq j} P_i^2 P_j^2 + A_{112} \sum_{i,j=1,2,3}^{i\neq j} P_i^4 P_j^2 \\ & + A_{123} P_1^2 P_2^2 P_3^2 \end{aligned} \tag{1}$$

where A_1, A_{11}, A_{111}, A_{12}, A_{112} and A_{123} are the Landau coefficients. Here only A_1 is assumed to be temperature(T) and defect concentration(c) dependent, i.e., $A_1 = A_1^0(T - T_C)$ whereA_1^0 is a constant. The gradient energy density f_{grad} is calculated by $f_{gradient} = \frac{1}{2}G_{11}(\sum_{i=1,2,3;j=1,2,3}(P_{i,j})^2)$, where G_{11} is the gradient energy coefficient. The electric energy density f_{elec} is decomposed into four parts: the dipole-dipole interaction energy density$f_{dipole} = -\frac{1}{2}E_iP_i$ (E_i is the inhomogeneous electric field caused by dipole-dipole interactions), the depolarization energy density $f_{depol} = -\frac{1}{2}E_{i,depol}\bar{P}_i$($E_{i,depol}$ represents the average depolarization field caused by surface charges and $\bar{P}_i$is the spatial average of the ith component of the polarization vector), the local electric energy density$f_{local} = -E_{i,local}P_i$($E_{i,local}$is the local electric field along the ith direction caused by point defects), and the energy density due to the applied external electric field $f_{appl} = -E_{i,appl}P_i$($E_{i,appl}$ is the applied electric field along the ith direction). The elastic energy density f_{elas} is calculated by $f_{elas} = \frac{1}{2}C_{ijkl}e_{ij}e_{kl} = \frac{1}{2}C_{ijkl}(\varepsilon_{ij} - \varepsilon_{ij}^0)(\varepsilon_{kl} - \varepsilon_{kl}^0)$, where$C_{ijkl}$is the elastic stiffness tensor, and e_{ij},$\varepsilon_{ij}$and ε_{ij}^0denote the elastic strain, total strain and spontaneous strain, respectively. The spontaneous strain is calculated by $\varepsilon_{ij}^0 = Q_{ijkl}P_kP_l$, where Q_{ijkl} is the electrostrictive coefficient of a single crystal.

The evolution of domain microstructure can then be obtained by solving the time-dependent Ginzburg-Landau equation:

$$\frac{\partial P_i(r,t)}{\partial t} = -M\frac{\delta F}{\delta P_i(r,t)}, i = 1,2,3 \tag{2}$$

where M is the kinetic coefficient and t is the time. The domain wall energy for 90° domain walls is assumed to be 0.01 J/m^2 [31], which yields a length scale l_0 of ~5 nm. The simulation cell sizes are 512 × 512(two dimensional(2D)), which corresponds to a system with size of $\sim 2.5 \times 2.5\mu m$. Periodic boundary condition is applied along both dimensions. The following parameters are adopted in the current simulations: 1) Landau parameters, which are modified from those of $BaTiO_3$ [32]: $A_1^0 = 0.0035 \times 10^8 C^{-2}m^2N$, $A_{11} = -3.697 \times 10^8 C^{-4}m^6N$, $A_{111} = 82.94 \times 10^8 C^{-6}m^{10}N$, $A_{12} = 1.625 \times 10^8 C^{-4}m^6N$, $A_{112} = 447 \times 10^8 C^{-6}m^{10}N$, $A_{123} = 691 \times 10^8 C^{-6}m^{10}N$, $T_c^{00} = 120^oC$. 2) electrostrictive coefficient and elastic constant(in the Voigt notation), which adopt those of $BaTiO_3$ [33,34]:$C_{11} = 1780 \times 10^8 m^{-2}N$, $C_{12} = 964 \times 10^8 m^{-2}N$, $C_{44} = 1220 \times 10^8 m^{-2}N$, $Q_{11} = 0.1 \times 10^7 C^{-2}m^2N$, $Q_{12} = -0.034 \times 10^7 C^{-2}m^2N$, $Q_{44} = 0.029 \times 10^7 C^{-2}m^2N$. 3) the parameter characterizing the strength of the local-field effect(λ), i.e., the increase of the magnitude of local electric field with the increase

of $c(\lambda=|E_{local}|/c)$: λ=200 kV/cm, which is in a reasonable range according to references [28]. 4) the parameter characterizing the strength of the local-T_C effect(b), i.e., the slope of the decrease of T_C with increase of $c(b=-dT_C/dc)$: b = 700 °C. For references, b∼500 °C for $BaZr_cTi_{1-c}O_3$ system [25], b∼700 °C for $BaSn_cTi_{1-c}O_3$ system, [23] b∼2100 °C for $(La_cPb_{1-c})(Zr_{0.4}Ti_{0.6})_{1-c/4}O_3$ system [24], b∼600 °C for PT-cPMN system [26]. These parameters are then reduced to a dimensionless form to simplify calculations [35].

The heat capacity is calculated through $C=-T(\frac{\partial^2 F}{\partial T^2})$. The *P-E* and *S-E* loops are calculated by measuring the polarization and strain of the system during the process of applying an external electric field. For the zero-field-cooling (ZFC) samples, the sample is first cooled under zero external electric field and then heated under a small constant external electric field(∼6.5 kV/cm). For the field-cooling (FC) sample, the sample is first cooled and then heated under a small constant external electric field(∼6.5 kV/cm). The polarization is measured during field heating process for both the ZFC and FC curves. The $P_{m,local}$∼T curves are obtained by selecting the maximum polarization among all grid points in the system at different temperatures. The dielectric permittivity vs T curves at different frequencies are calculated by recording the polarization change of the system under a small AC electric field during multiple cycles. The volume fraction of the paraelectric phase (V_{para}) at different temperatures are calculated by the number of grid points which has P<0.05C/m^2 divided by the total number of grid points. Correspondingly, the volume fraction of polar nanodomains (V_{pnd}) are obtained by counting the number of grid points which has $P_1 > P_0$ or $P_2 > P_0$ (P_0 is set to be a value at the jump of $P_{m,local}$∼T curve upon cooling for each defect concentration) and dividing it by the total number of grid points. The volume fraction of polar nanoregions (V_{pnr}) are calculated by V_{pnr} =1-V_{para} -V_{pnd}.

3. Results and Discussions

3.1. The change of domain structure and property from normal ferroelectrics to relaxor as induced by point defects doping

The evolution of the ferroelectric domain structure with temperature at three representative average defect concentrations ($\bar{c}$=0, 0.2, and 0.4) is shown in Fig. 2(a) (See Supplementary Figure S1 for those of all studied concentrations). It is seen that when defect concentration increases, the normal ferroelectric transforms to relaxor ferroelectric characterized by the nanodomain structures, which is consistent with the experimental observations [4–5]. The temperature dependences of the normalized heat capacity at different defect concentrations are calculated and the result are shown in Fig. 2(b), [3] which illustrates that the normal ferroelectric with an obvious heat capacity peak transforms to a relaxor without detectable heat capacity peak at about $\bar{c} > 0.1$. In addition, the polarization-electric field (*P-E*) and strain-electric field (*S-E*) loops at T = 10 °C are also calculated (see Fig. 2(c) and 2(d)). In addition to the nanodomain structures shown in Fig. 2(a) and the absence of the heat capacity peak shown in Fig. 2(b), the *P-E* and *S-E* loops become slim with small hysteresis at $\bar{c} > 0.1$, which are all unique characteristics of relaxors [17]. This further confirms that relaxor appears at $\bar{c} > 0.1$.

3.2. Prediction of the three characteristic temperatures (T_B, T^* and T_f) for relaxor ferroelectrics

Before determining the three characteristic temperatures (T_B, T^* and T_f) through our phase field simulations, first we need to know how the three characteristic temperatures are detected in experiments. In experiments T_B can be detected by the temperature below which the refractive index shows an anomaly, which corresponds to the nonzero value of the sum of the quadratic function of local polarization [20,36]. On the other hand, T^* can be detected experimentally by the temperature at which the acoustic emission shows a peak, which corresponds to a local structure change or a local phase transition [21,22]. Finally, T_f can be detected by the peak temperature of ZFC curve [37] or can be approximated by fitting the Vogel-Fulcher law based on the dielectric permittivity-temperature spectrum at different frequencies [38].Here in the phase field simulations, we define T_B as the temperature at which the local polarization reaches a cut-off non-zero value(0.05C/m^2)(i.e., assuming that only local polarization larger than the cut-off value can be detected by the refractive index anomaly), T^* as the temperature at which the ZFC/FC curve begins to split as an indication of local ferroelectric transition [18], and T_f as the peak temperature of the ZFC curve. Note that changing the cut-off value or changing the magnitude of external electric field exerted for calculating ZFC/FC curves would slightly change the absolute value of T_B, T^* and T_f for each sample, however, the variation tendency of them with average defect concentration would not vary much.

Fig. 3(a) plots the maximum local polarization ($P_{m,local}$) versus T curve of a representative relaxor composition $\bar{c}$=0.4. It is seen that $P_{m,local}$ has three distinctive slopes: with decreasing temperature it first increases slowly, followed by a sharp jump from a relatively small value to a relatively large value within a narrow temperature range, and then resumes a gradual increase again. Such tendency is consistent with that computed by first-principles for $PbTiO_3$-xPMN (PT-xPMN) relaxor [39]. As mentioned above, we use a cut-off non-zero value of $P_{m,local}$ = 0.05C/m^2 to define the characteristic temperature T_B in our study. It is ∼190 °C for $\bar{c}$=0.4. The sharp increase in $P_{m,local}$ at ∼70 °C indicates a local ferroelectric phase transition, suggesting that the intermediate temperature T^* would appear nearby this drastic increase. To detect T^* as well as the freezing temperature T_f, we calculate the zero-field cooling and field cooling (ZFC/FC) curves for $\bar{c}$=0.4 and the results are shown Fig. 3(b). As mentioned above, T^* can be defined in the ZFC/FC curve as the temperature at which the ZFC/FC curves begin to split, which is ∼10 °C (see the inset in Fig. 3(b), where δ_P(ZFC-FC) is the difference between polarization on ZFC and FC curves). T_f is approximated by the peak in the ZFC curve [40,41], which is ∼ −170 °C. In addition, the dielectric permittivity-T spectrum at different frequencies is also calculated for $\bar{c}$=0.4 relaxor as shown in Fig. 3(c) and by fitting the Vogel-Fulcher law, T_f is approximated to be −169 °C, which is close to the value obtained by the ZFC curve. Thus, all the three characteristic temperatures for $\bar{c}$ = 0.4 relaxor (T_B=190 °C, T^*=10 °C, T_f∼−170 °C) have been detected.

A phase diagram can be constructed based on the $P_{m,local}$ ∼T curves and ZFC/FC curves for all compositions ($\bar{c}$= 0 − 0.5)(See Supplementary Fig. S2), as illustrated in Fig. 4(a). When the average defect concentration $\bar{c}$ increases, the normal ferroelectrics change to relaxor ferroelectrics. For relaxor compositions ($\bar{c} > 0.1$), when $\bar{c}$ increases, T_B varies slightly, while T^* and T_f decrease more significantly. These predictions qualitatively agree with the variation tendencies of these three characteristic temperatures with defect concentration reported in experiments for PT-xPMN relaxor, [19,21] as illustrated in Fig. 4(b), and PT-xPbZn$_{1/3}$Nb$_{2/3}$O$_3$ (PT-xPZN) relaxor [42]. Note that changing the strength of local-field and local-T_C effect (λ and b) in the current model system would change the variation tendency of T_B,$T^*$and T_f. Fig. 5(a) demonstrates that as λ decreases from 200 kV/cm to 133 kV/cm and finally to 66 kV/cm (b is constant at 700 °C), T_B decreases while T^* and T_f almost keep constant. Fig. 6(b) demonstrates that as b decreases from 700 °C to 500 °C and finally to 300 °C (λ is constant at 200 kV/cm), T_B, T^* and T_f all increases. Therefore, how the three characteristic temperatures change with defect concentration depends on the balance between parameters λ and b. In PT-xPMN system, Mg^{2+} and Nb^{5+} (or $(Mg_{1/3}Nb_{2/3})^{4+}$) can be regarded as point defects substituting

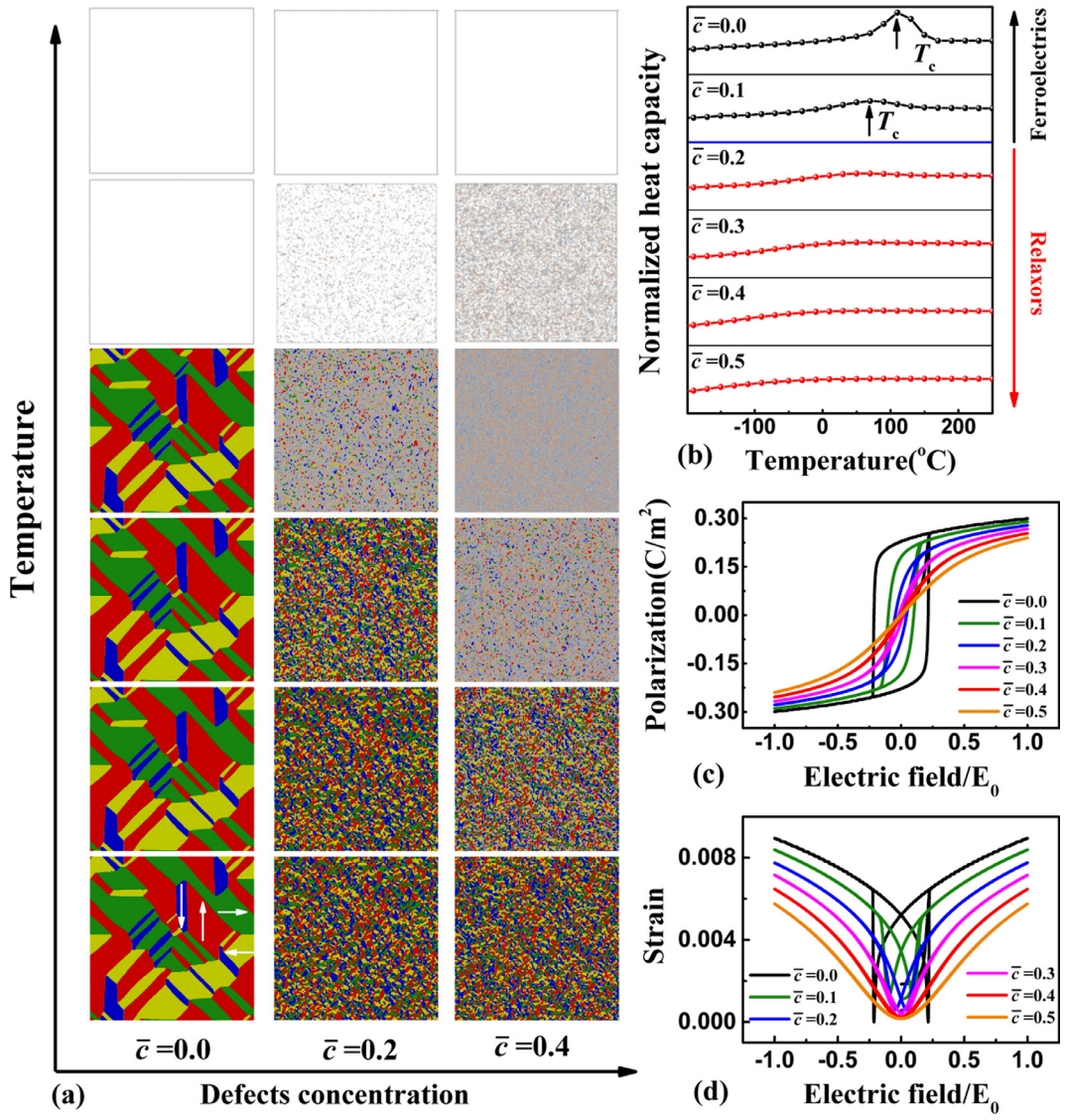

Fig. 2. (a) The domain structure evolution with temperature at three representative defect concentrations ($\bar{c}$=0, 0.2, 0.4). The arrows in the bottom-left figure indicates the polarization direction of different bright colors. The dim colors represent small polarization length with random directions. The white color represents the paraelectric region. (b) The normalized heat capacity-temperature curve for all concentrations. (c) The P-E loop of all $\bar{c}$at T = 10 °C, where E_0~650 kV/cm. (d) The S-E loop of all $\bar{c}$at T = 10 °C.

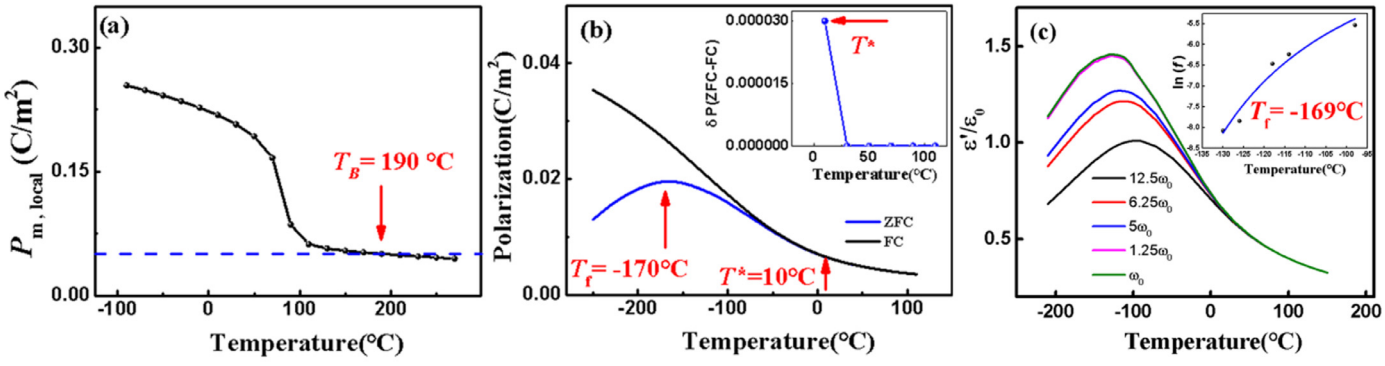

Fig. 3. Determination of three characteristic temperatures (T_B, T^*, and T_f) of $\bar{c}$ = 0.4 relaxor. (a) $P_{m,local}$ vs T curve, which defines T_B; (b) ZFC/FC curve, which defines T^* and T_f; (c) dielectric permittivity vs T curves at different frequencies, which can also define T_f.

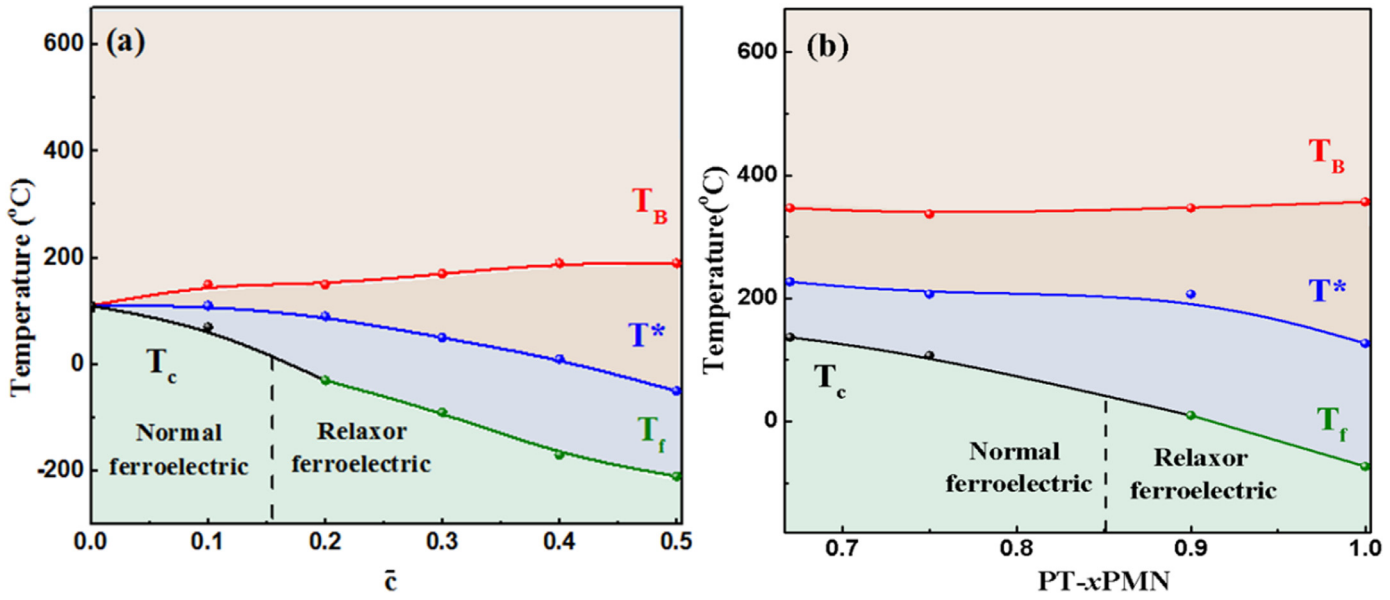

Fig. 4. (a) Calculated phase diagram of doped ferroelectric systems in the current simulations. (b) Experimental phase diagram of PT-*x*PMN system. [19·21].

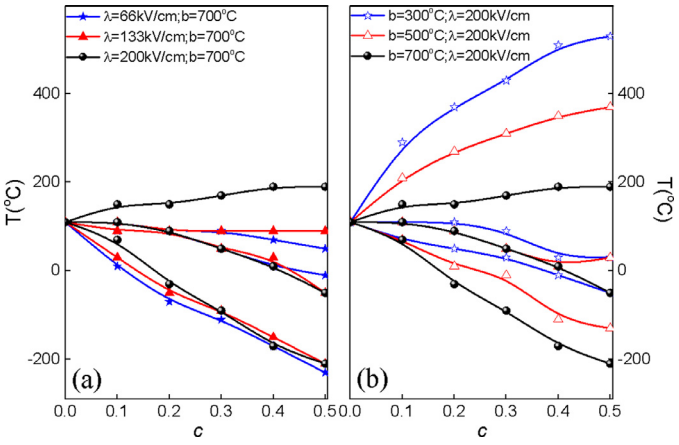

Fig. 5. (a) Variation of the three characteristic temperatures with the decrease of λ; (b) Variation of the three characteristic temperatures with the decrease of *b* .

Ti^{4+}. These point defects could produce relatively large local-field effect due to their heterovalent nature and they could also produce relatively large local-T_C effects due to the non-ferroelectric nature of Mg^{2+} defect. Thus, the variation tendency of the three characteristic temperatures with defect concentration in PT-*x*PMN system qualitatively resemble those predicted for the current model system with both large local-T_C effect and large local-field effect.

3.3. Role of local-field and local-T_C effect in the appearance of T_B and T^* in relaxors

To explore what are responsible for the appearance of T_B and T^* in relaxors, we carry out a controlled study by turning off respectively the local-field effect (Case 1, with localT_C effect only) and local-T_C effect (Case 2, with local electricfield effect only). The domain microstructures formed upon cooling at different $\bar{c}$ for case 1 and case 2 can be found in Supplementary Fig. S3 and S4. We find in both cases that the domain size decreases with increasing $\bar{c}$, suggesting that both effects can produce the nanodomain state of relaxors. In addition, the heat capacity-*T* spectrum as well as the *P-E* and *S-E* loop at different $\bar{c}$ demonstrate that the normal ferroelectrics turns to relaxors with $\bar{c}$ increases for both cases (See Supplementary Fig. S5 and S6). These results suggest that either local-T_C or local-field effect alone could produce the following features of relaxors: nanodomains, nondetectable heat capacity peak during the transition, and slim *P-E* and *S-E* loops.

However, by considering only one effect, not all three characteristic temperatures of a relaxor reported in experiments could be predicted. The $P_{m,local}$ versus *T* curves and the ZFC/FC curves for a representative relaxor ($\bar{c} = 0.4$) in the two cases of the controlled simulation study are plotted in Fig. 6(a1)−6(b1) and Fig. 6(a2)−6(b2), respectively. It is readily seen that in Case 1, $P_{m,local}$ jumps from zero to a large value upon cooling, and the ZFC and FC curves split well above T_f. Thus, in Case 1, T^* can be predicted but T_B could not be predicted. On the other hand, in Case 2, $P_{m,local}$ gradually increases from nearly zero to the cut-off value ($0.05C/m^2$), which thus defines T_B. However, unlike Case 1, the $P_{m,local}$ - *T* curve does not exhibit any abrupt jump during the entire cooling process, thus there is no indication of abrupt local ferroelectric transition. In addition, the ZFC/FC curves shown in Fig. 6(b2) splits at a temperature close to T_f, which may not be defined as T^* because T^* should be much higher than T_f or T_C as found in experiments. [21,43]. Thus, in Case 2, T_B can be predicted but T^* cannot be well defined [44]. Fig. 6(a3) and 6(b3) show the $\bar{c}$-*T* phase diagram of the doped ferroelectric system for Case 1 and Case 2, respectively (See Supplementary Fig. S7 and S8) [45]. It is clear that the local-T_C and local-field effect of point defects contributes to the appearance of T^* and T_B in relaxors, respectively. Moreover, compared to the phase diagram given in Fig. 4(a) in which both effects are considered, T_B in Fig. 6(b3) is much higher. This is because when both local-T_C and local-field effects are considered, at local regions with high electric fields (i.e., large local *c*), the local T_C is much lower than the average T_C, thus local polarization is more difficult to be induced by electric fields and T_B would decrease.

The reason why T_B is associated with the local-field effect and T^* is associated with the local T_C-effect can be explained by considering the Landau free energy shown schematically in Fig. 6(a4) and 6(b4). The local-T_C effect indicates that at a temperature above the average T_C of the whole system(for example, at T^*), when the local defect concentration *c* is smaller than $\bar{c}$, a local ferroelectric transition could occur because according to the Landau free energy

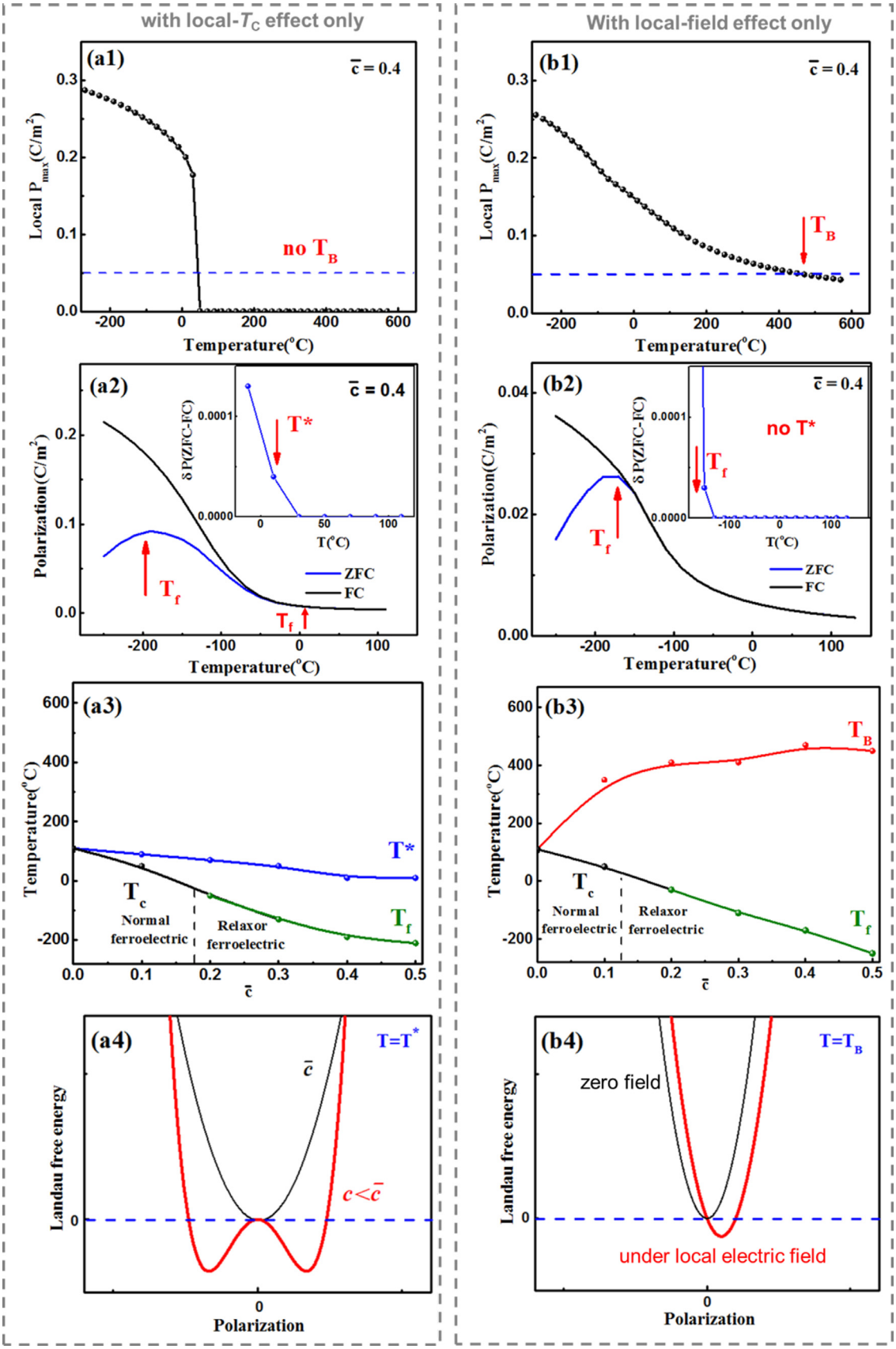

Fig. 6. Effect of local *Tc* and local field on the formation of relaxors. $P_{m,local}$ vs *T* curve for $\bar{c}$= 0.4 at Case 1(a1) and Case 2(b1); ZFC/FC curve for $\bar{c}$= 0.4at Case 1(a2) and Case 2(b2); $\bar{c}$-*T* phase diagram at Case 1(a3) and Case 2(b3); the schematic Landau free energy change at Case 1(a4) and Case 2(b4).

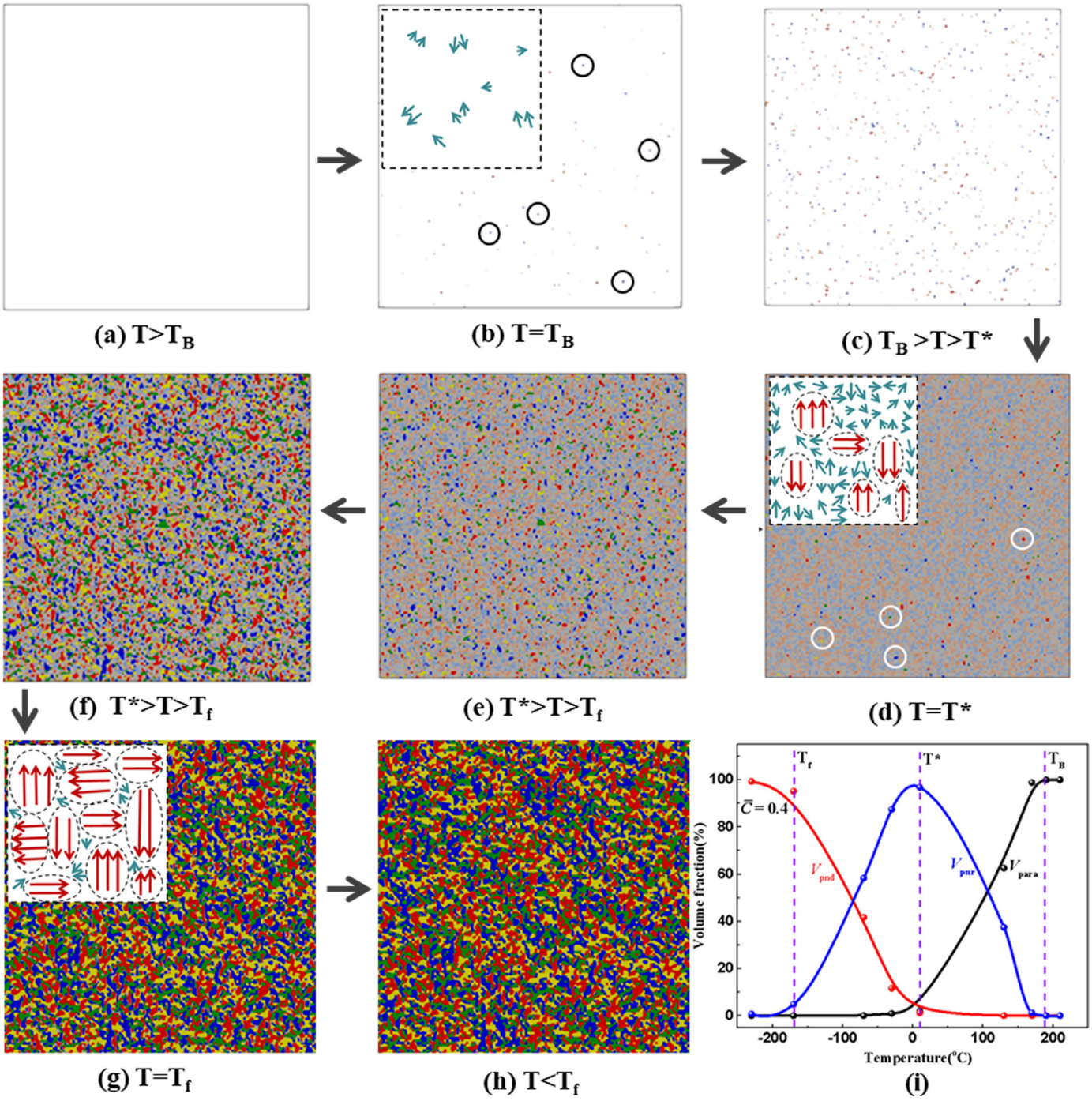

Fig. 7. (a)-(h) Domain structure evolution with temperature decreasing near the three characteristic temperatures of $\bar{c} = 0.4$ relaxor when both local-field and local-T_C effect are considered. The white, dim and bright colors indicate the paraelectric region, PNRs and PNDs, respectively. The black circles in (b) denote several examples of PNRs. The white circles in (d) denote four representative PNDs with directions illustrated in the bottom-left figure of Fig. 1(a). The insets in (b), (d), and (g) schematically show the polarization direction, polarization length and volume fraction of PNRs and PNDs at T_B, T^* and T_f, respectively. (i) The change of volume fraction of paraelectric regions (V_{para}), PNRs (V_{pnr}), and PNDs (V_{pnd}) with temperature for $\bar{c} = 0.4$ relaxor.

shown in Fig. 6(a4), the ferroelectric phase rather than the paraelectric phase is stable in that local region. Such ferroelectric transition induced local polarization is relatively large. On the other hand, the local electric field can induce polarization change of the paraelectric phase by shifting the Landau free energy as illustrated in Fig. 6(b4). The induced polarization would be small and not detectable at temperatures above T_B. As the temperature decreases to T_B and below, the curvature of the free energy curve at the paraelectric phase ($\boldsymbol{P} = 0$) becomes smaller and the induced polarization under local electric field becomes apparent and detectable by experimental tools.

The variation tendency of the three characteristic temperatures on λ and b as demonstrated in Fig. 5(a) and 5(b) can then be explained. Firstly, why T_B decreases as λ decreases? This is because if the strength of local-field decreases(λ decreases), then the curvature of the Landau free energy has to become smaller by lowering the temperature in order to induce a detectable polarization. Secondly, why T_B increases as b decreases? This is because if T_C in-

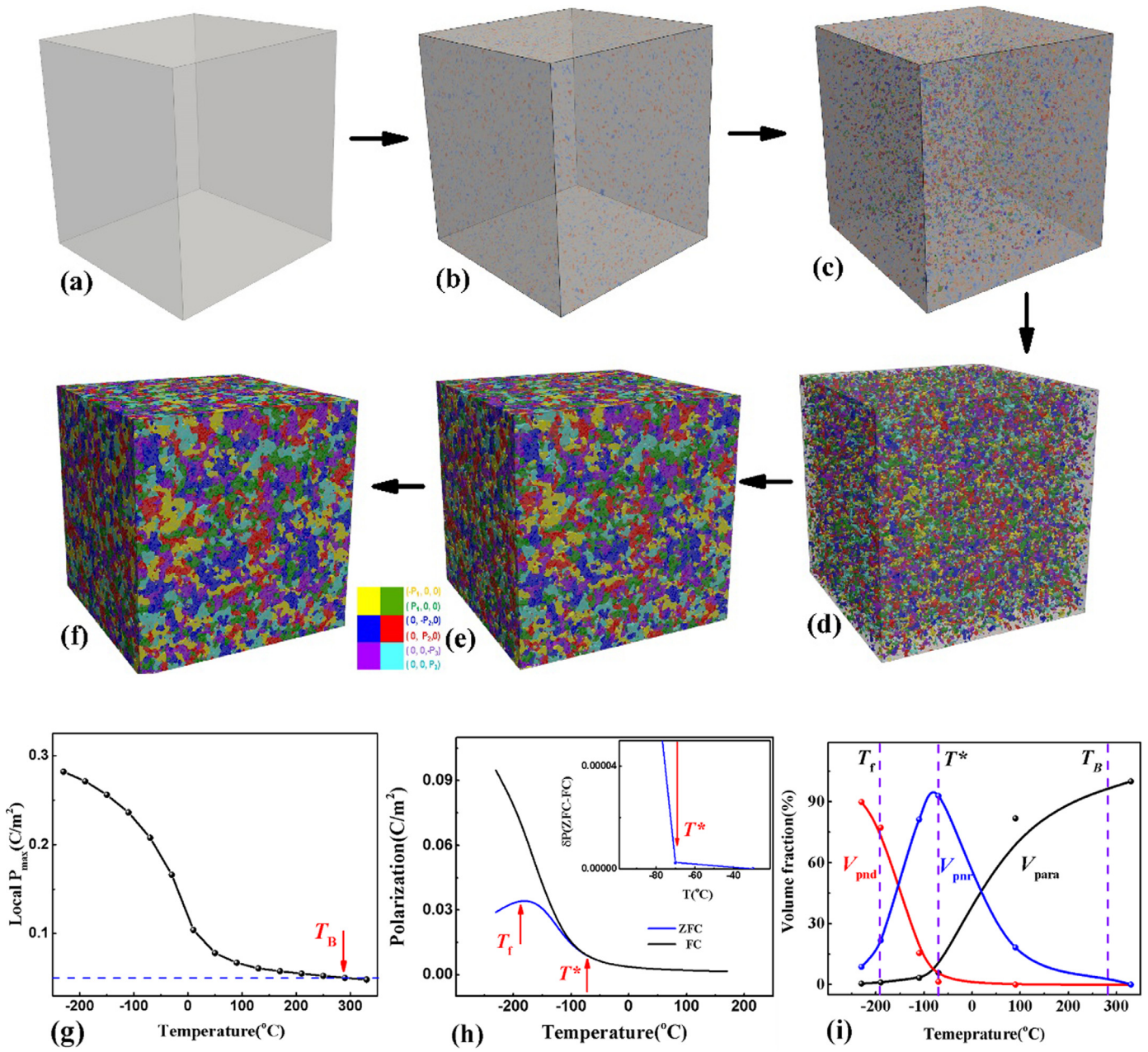

Fig. 8. (a)-(f) The 3D domain structure evolution with temperature decreasing at $\bar{c} = 0.4$with both local-T_c effect and local-field effect considered. (a) $T>T_B$; (b) $T^*<T<T_B$;(c) $T = T^*$; (d)$T_f<T<T^*$; (e)$T=T_f$; (f) $T<T_f$. (g) The corresponding $P_{m,local}$ ~T curve. (h) The corresponding ZFC/FC curves. (i) Variation of volume fraction of paraelectric phase (V_{para}), PNRs (V_{pnr}) and PNDs (V_{pnd}) with temperature.

creases (b decreases), then the curvature of the Landau free energy becomes small enough at a higher temperature and a detectable polarization can be induced by the local electric field. Finally, why T^* and T_f increase as b decreases? This is because if if T_C increases (b decreases), then both the local and global ferroelectric phase transition can occur at higher temperature.

3.4. Domain structure evolution process at the three characteristic temperatures (T_B, T^* and T_f) of relaxor ferroelectrics

The detailed domain microstructure evolution during cooling near T_B, T^* and T_f of a relaxor with $\bar{c} = 0.4$ when both local-field and local-T_C effects are considered (the last column in Fig. 2(a)) is analyzed in Fig. 7. At $T>T_B$ (Fig. 7(a)), the material is paraelectric without detectable polarization ($P_{m,local}$ is smaller than the cut-off value). At $T=T_B$ (Fig. 7(b)), nanoregions with small polarization length and random directions (named as polar nanoregions (PNRs), which are distorted paraelectric phase induced by local-field effect) appear in the paraelectric matrix (see the circled regions in Fig. 7(b)). The nanoregions are polar but not ferroelectric yet and thus cannot be called ferroelectric nanodomains [19]. At $T^*<T<T_B$ (Fig. 7(c)), the volume fraction of such nanoregions gradually increases at the expense of the paraelectric matrix. With temperature further decreasing down to T^*(Fig. 7(d)), tetragonal ferroelectric nanodomains with large polarization length (named as polar nanodomains (PNDs), [19] which correspond to local ferroelectric transition induced by local-T_C effect) start to appear (see the white circles in Fig. 7(d)). Below T^*(Fig. 7(e) and 7(f)), the volume fraction of PNDs gradually increases at the expense of PNR, and at T_f (Fig. 7(g)), the majority of the system is occupied by PNDs.

With temperature further decreasing to below T_f (Fig. 7(h)), the nanodomain structure does not show any obvious changes. Variations of the volume fractions of the paraelectric regions (V_{para}), PNR (V_{pnr}), as well as PND (V_{pnd}) in the system with temperature for $\bar{c} = 0.4$ relaxor during the above evolution process are plotted in Fig. 7(i) (See Supplementary Fig. S9 for the variation of volume fractions for other compositions).

Note that here the PNR and PND are all static and thus are different from the dynamic and static domains in references [39,46]. The fundamental difference between PNR and PND is that PNR refers to nanoregions with distorted paraelectric phase(as schematically shown in Fig. 6(b4)) and PND refers to nanoregions with true ferroelectric phase(as schematically shown in Fig. 6(a4)).

3.5. 3D simulation results

The above simulations are performed in 2D. In 3D, similar results can be obtained. Fig. 8(a)-(f) illustrated the 3D simulation results of domain structure evolution upon cooling at $\bar{c} = 0.4$ when both local-T_C and local-field effects are considered. It is illustrated that similar to 2D cases, first PNRs with small polarization lengths appear and then PNDs with large polarization lengths occur. Fig. 8(g) and(h) shows the $P_{m,local}$ versus T curves and the ZFC/FC curves of $\bar{c} = 0.4$ relaxor, respectively, from which T_B, T^* and T_f can be well defined. Fig. 8(i) plots the variation of V_{para}, V_{pnr}, and V_{pnd} with temperature upon cooling, which demonstrates similar evolution process as those illustrated for 2D cases as given in Fig. 7.

3.6. Implications for the origin of other ferroic glass and the designing strategy of relaxor ferroelectrics

This work clearly demonstrates that the local-field effect is responsible for the appearance of PNRs at T_B and the local-T_C effect is responsible for the appearance of PNDs at T^*. Note that our model could describe almost all relaxor systems and the difference between different relaxor systems lie in the different strengths of the local-T_C and local-field effects (parameter λ and b). For example, in ferroelectrics doped with non-ferroelectric isovalent ions such as $BaZr_xTi_{1-x}O_3$ and $BaSn_xTi_{1-x}O_3$ system, [47,48] the local-electric-field effect would be small while the local-T_C effect could be strong [15]. On the other hand, in ferroelectrics doped with ferroelectric heterovalant ions such as $BaTiO_3$-$KNbO_3$ system, [49] the local-T_C effect would be small while the local-electric-field effect would be large.

The above mechanism could also shed light on the physical origin of spin glass in ferromagnetic systems [50] and strain glass in ferroelastic systems [51], both of which are physically parallel to relaxors and belong to ferroic glasses along with relaxors [52]. In addition, this work could guide the future design of relaxors with desired properties. For example, it has been reported that relaxors between T_B and T^* normally exhibits large electrostrictive strain and thus could be utilized in electrostrictive devices [17,53]. Thus, by selectively choosing dopants with large local-field effect and small local-T_C effect(as the case when b = 300 °C,λ=200 kV/cm shown in Fig. 6(b)), relaxors with a large (T_B-T^*) value could be obtained and thus large electrostrictive strain in a wide temperature range could be realized.

4. Conclusions

In conclusions, we have illustrated that by considering both the local T_C variation and local electric field caused by random distribution of point defects, our phase field simulations predict all three characteristic temperatures T_B, T^* and T_f well defined in relaxors. A defect concentration-temperature phase diagram of the doped ferroelectric system has been constructed by considering both effects, which is consistent with the experimental results. We find that the local-field effect is responsible for the appearance of T_B, at which detectable polarization is induced in the paraelectric phase by the local electric field of point defects, while the local-T_C effect is responsible for the appearance of T^*, at which local ferroelectric phase transition occurs. Detailed microstructure changes in relaxors with decreasing temperature have been documented. This work unravels the roles of point defects in the formation of relaxors and its unique behaviors in terms of the individual and combined roles played by the local-T_C and local-field effects associated with point defects. It could shed light on the physical mechanism of ferroic glass and could guide the design of relaxors with tailored properties through fine-tuning the local-T_C and local-field effects by selectively doping different types of point defects.

Declaration of Competing Interest

The authors declare that they have no known competing financial interests or personal relationships that could have appeared to influence the work reported in this paper.

Acknowledgement

Z.H., X.K., D.W., S.Y. and X.R. acknowledges the support from the National Natural Science Foundation of China (Grant No. 51802249, No. 11672222, No. 51801145, and No. 91963111), Key Scientific and Technological Innovation Team of Shaanxi province (2020TD-001), Innovation Capability Support Program of Shaanxi (No. 2018PT-28, 2017KTPT-04), the Fundamental Research Funds for the Central Universities (China), the World-Class Universities (Disciplines), the Characteristic Development Guidance Funds for the Central Universities, and “H2” High-Performance Cluster of XJTU. Y.W. acknowledges the support from US National Science Foundation (Grant No. DMR-1923929).

Supplementary materials

Supplementary material associated with this article can be found, in the online version, at doi:10.1016/j.actamat.2021.117558.

References

[1] K. Uchino, Ferroelectric Devices, Marcel Dekker, New York, 2000.
[2] S. Zhang, F. Li, X. Jiang, J. Kim, J. Luo, X. Geng, Advantages and challenges of relaxor-$PbTiO_3$ ferroelectric crystals for electroacoustic transducers – a review, Prog. Mater. Sci. 68 (2015) 1–66.
[3] F. Li, M.J. Cabral, B. Xu, Z. Cheng, E.C. Dickey, J.M. LeBeau, J. Wang, J. Luo, S. Taylor, W. Hackenberger, L. Bellaiche, Z. Xu, L.-.Q. Chen, T.R. Shrout, S. Zhang, Giant piezoelectricity of Sm-doped $Pb(Mg_{1/3}Nb_{2/3})O_3$-$PbTiO_3$ single crystals, Science 364 (2019) 264–268.
[4] X. Dai, A. DiGiovanni, D. Viehland, Dielectric properties of tetragonal lanthanum modified lead zirconate titanate ceramics, J. Appl. Phys. 74 (1993) 3399–3405.
[5] Z. Yu, C. Ang, R. Guo, A.S. Bhalla, Dielectric properties of $Ba(Ti_{1-x}Zr_x)O_3$ solid solutions, Mater. Lett. 61 (2007) 326–329.
[6] Z.-Y. Cheng, R.S. Katiyar, X. Yao, A.S. Bhalla, Temperature dependence of the dielectric constant of relaxor ferroelectrics, Phys. Rev. B 57 (1998) 8166.
[7] T. Roncal-Herrero, J. Harrington, A. Zeb, S.J. Milne, A.P. Brown, Nanoscale compositional segregation and suppression of polar coupling in a relaxor ferroelectric, Acta Mater 158 (2018) 422–429.
[8] D. Fu, H. Taniguchi, M. Itoh, S.-.Y. Koshihara, N. Yamamoto, S. Mori, Relaxor $Pb(Mg_{1/3}Nb_{2/3})O_3$: a Ferroelectric with Multiple Inhomogeneities, Phys. Rev. Lett. 103 (2009) 207601.
[9] D. Sherrington, BZT: a Soft Pseudospin Glass, Phys. Rev. Lett. 111 (2013) 227601.
[10] R. Blinc, J. Dolinsek, A. Gregorovic, B. Zalar, C. Filipic, Z. Kutnjak, A. Levstik, R. Pirc, Local polarization distribution and edwards-anderson order parameter of relaxor ferroelectrics, Phys. Rev. Lett. 83 (1999) 424.
[11] A.R. Akbarzadeh, S. Prosandeev, E.J. Walter, A. Al-Barakaty, L. Bellaiche, Finite-temperature properties of $Ba(Zr,Ti)O_3$ Relaxors from first principles, Phys. Rev. Lett. 108 (2012) 257601.
[12] J. Toulouse, B.E. Vugmeister, R. Pattnaik, Collective Dynamics of Off-Center Ions in $K_{1-x}Li_xTaO_3$: a model of relaxor behavior, Phys. Rev. Lett. 73 (1994) 3467.

[13] D. Sherrington, $Pb(Mg_{1/3}Nb_{2/3})O_3$: a minimal induced-moment soft pseudospin glass perspective, Phys. Rev. B 89 (2014) 064105.
[14] S. Tinte, B.P. Burton, E. Cockayne, U.V. Waghmare, Origin of the Relaxor State in $Pb(B_xB'_{1-x})O_3$ perovskites, Phys. Rev. Lett. 97 (2006) 137601.
[15] D. Phelan, C. Stock, J.A. Rodriguez-Rivera, S. Chi, J. Leão, X. Long, Y. Xie, A.A. Bokov, Z.-G. Ye, P. Ganesh, P.M. Gehring, Role of random electric fields in relaxors, PNAS 111 (2014) 1754–1759.
[16] W. Kleemann, Random fields in relaxor ferroelectrics — a jubilee review, J. Adv. Dielectr. 2 (2012) 1241001.
[17] T. Li, C. Liu, X. Ke, X. Liu, L. He, P. Shi, X. Ren, Y. Wang, X. Lou, High electrostrictive strain in lead-free relaxors near the morphotropic phase boundary, Acta Mater 182 (2020) 39–46.
[18] D. Wang, X. Ke, Y. Wang, J. Gao, Y. Wang, L. Zhang, S. Yang, X. Ren, Phase diagram of polar states in doped ferroelectric systems, Phys. Rev. B 86 (2012) 054120.
[19] J. Toulouse, The three characteristic temperatures of relaxor dynamics and their meaning, Ferroelectrics 369 (2008) 203–213.
[20] G. Burns, F.H. Dacol, Crystalline ferroelectrics with glassy polarization behavior, Phys. Rev. B 28 (1983) 2527.
[21] B. Dkhil, P. Gemeiner, A. Al-Barakaty, L. Bellaiche, E. Dul'kin, E. Mojaev, M. Roth, Intermediate temperature scale T* in lead-based relaxor systems, Phys. Rev. B 80 (2009) 064103.
[22] E. Dul'kin, M. Roth, P.-.E. Janolin, B. Dkhil, Acoustic emission study of phase transitions and polar nanoregions in relaxor-based systems: application to the $PbZn_{1/3}Nb_{2/3}O_3$ family of single crystals, Phys. Rev. B 73 (2006) 012102.
[23] Y.G. Yao, C. Zhou, D. Lv, D. Wang, H. Wu, Y. Yang, X. Ren, Large piezoelectricity and dielectric permittivity in $BaTiO_3$-x$BaSnO_3$ system: the role of phase coexisting, EPL 98 (2012) 27008.
[24] Z.M. Sun, D. Xue, H. Wu, Y. Ji, X. Ding, D. Wang, Y. Yang, X. Ren, Time-dependent ferroelectric transition in $Pb_{(1-x)}(Zr_{0.4}Ti_{0.6})_{(1-x/4)}O_3$-xLa system, Appl. Phys. Lett. 102 (2013) 222907.
[25] T. Maiti, R. Guo, A.S. Bhalla, Evaluation of experimental resume of $BaTi_{1-x}Zr_xO_3$ with perspective to ferroelectric relaxor family: an Overview, Ferroelectrics 425 (2011) 4–26.
[26] M.J. Krogstad, P.M. Gehring, S. Rosenkranz, R. Osborn, F. Ye, Y. Liu, J.P.C. Ruff, W. Chen, J.M. Wozniak, H. Luo, O. Chmaissem, Z.-G. Ye, D. Phelan, The relation of local order to material properties in relaxor ferroelectrics, Nature Materi. 17 (2018) 718–724.
[27] M.D. Glinchuk, R. Farhi, A random field theory based model for ferroelectric relaxors, J. Phys.:Condens. Matter 8 (1996) 6985–6996.
[28] S. Wang, M. Yi, B.X. Xu, A phase-field model of relaxor ferroelectrics based on random field theory, Int. J. Solid. Struct. 83 (2016) 142–153.
[29] S. Choudhury, Y.L. Li, C.E. Krill III, L.-.Q. Chen, Phase-field simulation of polarization switching and domain evolution in ferroelectric polycrystals, Acta Mater 53 (2005) 5313–5321.
[30] X.Q. Ke, D. Wang, X. Ren, Y. Wang, Formation of monoclinic nanodomains at the morphotropic phase boundary of ferroelectric systems, Phys. Rev. B 88 (2013) 214105.
[31] J. Hlinka, Ferroelectrics 349 (2007) 49.
[32] Y.L. Li, L.E. Cross, L.Q. Chen, A phenomenological thermodynamic protential for $BaTiO_3$ single crystals, J. Appl. Phys. 98 (2005) 064101.
[33] J. Hlinka, P. Márton, Phenomenological model of a 90°domain wall in $BaTiO_3$-type ferroelectrics, Phys. Rev. B 74 (2006) 104104.
[34] J.J. Wang, F.Y. Meng, X.Q. Ma, M.X. Xu, L.Q. Chen, Lattice, elastic, polarization, and electrostrictive properties of BaTiO3 from frist-principles, J. Appl. Phys 108 (034107) (2010).
[35] D. Wang, S. Hou, Y. Wang, X.D. Ding, S. Ren, X.B. Ren, Y.Z. Wang, Superelasticity of slim hysteresis over a wide temperature range by nanodomains of martensite, Acta Mater 66 (2014) 349–359.
[36] G. Burns, F.H. Dacol, Crystalline ferroelectrics with a glassy polarization phase, Jpn. J. Appl. Phys 24 (1985) 85–88.
[37] D. Viehland, J.F. Li, S.J. Jang, L.E. Cross, M. Wutting, Glassy polarization behavior of relaxor ferroelectrics, Phys. Rev. B 46 (1992) 8013.
[38] Y. Yang, Y.C. Ji, M.X. Fang, Z.J. Zhou, L. Zhang, X.B. Ren, Morphotropic relaxor boundary in a relaxor system showing enhancement of electrostrain and dielectric permittivity, Phys. Rev. Lett. 123 (2019) 137601.
[39] H. Takenaka, I. Grinberg, S. Liu, A.M. Rappe, Slush-like polar structures in single-crystal relaxors, Nature 391 (2017) 546.
[40] J.A. Mydosh, Spin Glasses: An Experimental Introduction, Taylor & Francis, London, 1993.
[41] D. Sherrington, A spin glass perspective on ferroic glasses, Phys. Status. Solidi B 251 (2014) 1967.
[42] M. Roth, E. Mojaev, E. Dulkin, P. Gemeiner, B. Dkhil, Phase transition at a nanometer scale detected by acoustic emission within the cubic phase $Pb(Zn_{1/3}Nb_{2/3})O_3-xPbTiO_3$ relaxor ferroelectrics, Phys. Rev. Lett. 98 (2007) 265701.
[43] M. Roth, E. Mojaev, E. Dulkin, P. Gemeiner, B. Dkhil, Phase transition at a nanometer scale detected by acoustic emission within the cubic phase $Pb(Zn_{1/3}Nb_{2/3})O_3-xPbTiO_3$ relaxor ferroelectrics, Phys. Rev. Lett. 98 (2007) 265701.
[44] Note that *T*B was incorrectly defined in our previous study of the local-field effect on the formation of relaxors(reference 18).
[45] Note that in Fig. 4(a3), the boundary between normal ferroelectric and relaxor is approximately determined by the domain size at low temperature of each defect concentration.
[46] J. Hlinka, Do we need the ether of polar nanoregions? J. Adv. Dielectrics 2 (2012) 1241006.
[47] V.V. Shvartsman, J. Zhai, W. Kleemann, The Dielectric Relaxation in Solid Solutions $BaTi_{1-x}Zr_xO_3$, Ferroelectrics 379 (2009) 77–85.
[48] Y.B. Ma, C. Molin, V.V. Shavrtsman, S. Gebhardt, D.C. Lupascu, K. Albe, B.X. Xu, State transition and electrocaloric effect of Ba: simulation and experiment, J. Appl. Phys. 121 (2017) 024103.
[49] L. Zhang, X.J. Lou, D. Wang, Y. Zhou, Y. Yang, M. Kuball, M.A. Carpenter, X.B. Ren, Glass-Glass transitions by means of an acceptor-donor percolating electric-dipole network, Phys. Rev. Appl 8 (2017) 054018.
[50] J.A. Mydosh, Spin Glasses: An Experimental Introduction, Taylor & Francis, London, 1993.
[51] S. Sarkar, X. Ren, K. Otsuka, Evidence for strain glass in the Ferroelastic–Martensitic System $Ti_{50-x}Ni_{50+x}$, Phys. Rev. Lett. 95 (2005) 205702.
[52] D. Sherrington, A spin glass perspective on ferroic glasses, Phys. Status. Solidi B 251 (2014) 1967.
[53] F. Li, S. Zhang, D. Damjanovic, L.Q. Chen, T.R. Shrout, Local structural heterogeneity and electromechanical responses of ferroelectrics: learning from relaxor ferroelectrics, Adv. Func. Mater 28 (2018) 1801504.